Enhancing optofluidic actuation of micro-objets by tagging with plasmonic nanoparticles

Julien Burgin, Satyabrata Si, Marie-Hélène Delville, Jean-Pierre Delville

Enhancing optofluidic actuation of micro-objects by tagging with plasmonic nanoparticles

Julien Burgin,[1,2] Satyabrata Si,[3] Marie-Hélène Delville,[3] and Jean-Pierre Delville[1,2,*]

[1]Univ. Bordeaux, LOMA, UMR 5798, F-33400 Talence, France
[2]CNRS, LOMA, UMR 5798, F-33400 Talence, France
[3]CNRS, Univ. Bordeaux, ICMCB, 87 avenue du Dr. A. Schweitzer, Pessac, F-33608, France
**jp.delville@loma.u-bordeaux1.fr*

Abstract: We report experimentally and theoretically on the significant exaltation of optical forces on microparticles when they are partially coated by metallic nanodots and shined with laser light within the surface plasmon resonance. Optical forces on both pure silica particles and silica-gold raspberries are characterized using an optical chromatography setup to measure the variations of the Stokes drag versus laser beam power. Results are compared to the Mie theory prediction for both pure dielectric particles and core-shell ones with a shell described as a continuous dielectric-metal composite of dielectric constant determined from the Maxwell-Garnett approach. The observed quantitative agreement demonstrates that radiation pressure forces are directly related to the metal concentration on the microparticle surface and that metallic nanodots increase the magnitude of optical forces compared to pure dielectric particles of the same overall size, even at very low metal concentration. Behaving as "micro-sized nanoparticles", the benefit of microparticles coated with metallic nanodots is thus twofold: it significantly enhances optofluidic manipulation and motion at the microscale, and brings nanometric optical, chemical or biological capabilities to the microscale.

OCIS codes: (160.4236) Nanomaterials; (160.0160) Materials; (350.4855) Optical tweezers or optical manipulation; (290.4020) Mie theory; (280.7250) Velocimetry; (250.5403) Plasmonics.

References and links

1. A. Ashkin, "Optical trapping and manipulation of neutral particles using lasers," Proc. Natl. Acad. Sci. U.S.A. **94**(10), 4853–4860 (1997).
2. D. G. Grier, "A revolution in optical manipulation," Nature **424**(6950), 810–816 (2003).
3. A. Jonás and P. Zemánek, "Light at work: the use of optical forces for particle manipulation, sorting, and analysis," Electrophoresis **29**(24), 4813–4851 (2008).
4. A. A. Lall, A. Terray, and S. J. Hart, "On-the-fly cross flow laser guided separation of aerosol particles based on size, refractive index and density-theoretical analysis," Opt. Express **18**(26), 26775–26790 (2010).
5. S. J. Hart and A. V. Terray, "Refractive-index-driven separation of colloidal polymer particles using optical chromatography," Appl. Phys. Lett. **83**(25), 5316–5318 (2003).
6. S. J. Hart, A. V. Terray, and J. Arnold, "Particle separation and collection using an optical chromatographic filter," Appl. Phys. Lett. **91**(17), 171121 (2007).
7. T. Kaneta, Y. Ishidzu, N. Mishima, and T. Imasaka, "Theory of optical chromatography," Anal. Chem. **69**(14), 2701–2710 (1997).
8. R. W. Bowman and M. J. Padgett, "Optical trapping and binding," Rep. Prog. Phys. **76**(2), 026401 (2013).
9. R. W. Applegate, Jr., J. Squier, T. Vestad, J. Oakey, D. W. M. Marr, P. Bado, M. A. Dugan, and A. A. Said, "Microfluidic sorting system based on optical waveguide integration and diode laser bar trapping," Lab Chip **6**(3), 422–426 (2006).
10. M. P. MacDonald, G. C. Spalding, and K. Dholakia, "Microfluidic sorting in an optical lattice," Nature **426**(6965), 421–424 (2003).
11. M. Ploschner, T. Čižmár, M. Mazilu, A. Di Falco, and K. Dholakia, "Bidirectional optical sorting of gold nanoparticles," Nano Lett. **12**(4), 1923–1927 (2012).
12. A. S. Zelenina, R. Quidant, G. Badenes, and M. Nieto-Vesperinas, "Tunable optical sorting and manipulation of nanoparticles via plasmon excitation," Opt. Lett. **31**(13), 2054–2056 (2006).
13. A. Ashkin, J. M. Dziedzic, J. E. Bjorkholm, and S. Chu, "Observation of a single-beam gradient force optical trap for dielectric particles," Opt. Lett. **11**(5), 288–290 (1986).

14. K. Svoboda and S. M. Block, "Optical trapping of metallic Rayleigh particles," Opt. Lett. **19**(13), 930–932 (1994).
15. M. J. Guffey, R. L. Miller, S. K. Gray, and N. F. Scherer, "Plasmon-driven selective deposition of au bipyramidal nanoparticles," Nano Lett. **11**(10), 4058–4066 (2011).
16. J. R. Moffitt, Y. R. Chemla, S. B. Smith, and C. Bustamante, "Recent advances in optical tweezers," Annu. Rev. Biochem. **77**(1), 205–228 (2008).
17. M. Dienerowitz, M. Mazilu, and K. Dholakia, "Optical manipulation of nanoparticles: a review," J. Nanophotonics **2**(1), 021875 (2008).
18. H. Zhang and K. K. Liu, "Optical tweezers for single cells," J. R. Soc. Interface **5**(24), 671–690 (2008).
19. A. Ashkin and J. M. Dziedzic, "Optical trapping and manipulation of viruses and bacteria," Science **235**(4795), 1517–1520 (1987).
20. A. Terray, J. D. Taylor, and S. J. Hart, "Cascade optical chromatography for sample fractionation," Biomicrofluidics **3**(4), 044106 (2009).
21. J. S. Y. Kim, J. D. Taylor, H. D. Ladouceur, S. J. Hart, and A. Terray, "Radiation pressure efficiency measurements of nanoparticle coated microspheres," Appl. Phys. Lett. **103**(23), 234101 (2013).
22. R. R. Agayan, T. Horvath, B. H. McNaughton, J. N. Anker, and R. Kopelman, "Optical manipulation of metal-silica hybrid nanoparticles," Proc. SPIE **5514**, 502–513 (2004).
23. M. Rodriguez-Otazo, A. Augier-Calderin, and J. P. Galaup, "Nanometer gold–silica composite particles manipulated by optical tweezers," Opt. Commun. **282**(14), 2921–2929 (2009).
24. I. Choi, H. D. Song, S. Lee, Y. I. Yang, T. Kang, and J. Yi, "Core-satellites assembly of silver nanoparticles on a single gold nanoparticle *via* metal ion-mediated complex," J. Am. Chem. Soc. **134**(29), 12083–12090 (2012).
25. S. Balint, M. P. Kreuzer, S. Rao, G. Badenes, P. Miskovsky, and D. Petrov, "Simple route for preparing optically trappable probes for surface-enhanced Raman scattering," J. Phys. Chem. C **113**(41), 17724–17729 (2009).
26. R. Tamoto, S. Lecomte, S. Si, S. Moldovan, O. Ersen, M. H. Delville, and R. Oda, "Gold nanoparticle deposition on silica nanohelices: a new controllable 3d substrate in aqueous suspension for optical sensing," J. Phys. Chem. C **116**(43), 23143–23152 (2012).
27. S. Mühlig, C. Rockstuhl, V. Yannopapas, T. Bürgi, N. Shalkevich, and F. Lederer, "Optical properties of a fabricated self-assembled bottom-up bulk metamaterial," Opt. Express **19**(10), 9607–9616 (2011).
28. N. Engheta, "Circuits with light at nanoscales: optical nanocircuits inspired by metamaterials," Science **317**(5845), 1698–1702 (2007).
29. M. R. Jones, K. D. Osberg, R. J. Macfarlane, M. R. Langille, and C. A. Mirkin, "Templated techniques for the synthesis and assembly of plasmonic nanostructures," Chem. Rev. **111**(6), 3736–3827 (2011).
30. A. Tao, S. Habas, and P. Yang, "Shape control of colloidal metal nanocrystals," Small **4**(3), 310–325 (2008).
31. I. Pastoriza-Santos, D. Gomez, J. Pérez-Juste, L. M. Liz-Marzán, and P. Mulvaney, "Optical properties of metal nanoparticle coated silica spheres: a simple effective medium approach," Phys. Chem. Chem. Phys. **6**, 5056–5060 (2004).
32. T. Pham, J. B. Jackson, N. J. Halas, and T. R. Lee, "Preparation and characterization of gold nanoshells coated with self-assembled monolayers," Langmuir **18**(12), 4915–4920 (2002).
33. D. Blair and E. Dufresne, "The matlab particle tracking code repository," *http://physics.georgetown.edu/matlab/index.html*.
34. K. Nozawa, H. Gailhanou, L. Raison, P. Panizza, H. Ushiki, E. Sellier, J. P. Delville, and M. H. Delville, "Smart control of monodisperse Stöber silica particles: effect of reactant addition rate on growth process," Langmuir **21**(4), 1516–1523 (2005).
35. K. Nozawa, M. H. Delville, H. Ushiki, P. Panizza, and J. P. Delville, "Growth of monodisperse mesoscopic metal-oxide colloids under constant monomer supply," Phys. Rev. E Stat. Nonlin. Soft Matter Phys. **72**(1 Pt 1), 011404 (2005).
36. G. Frens, "Controlled Nucleation for the regulation of the particle size in monodisperse gold suspensions," Nature **241**, 20–22 (1973).
37. S. Basu, S. K. Ghosh, S. Kundu, S. Panigrahi, S. Praharaj, S. Pande, S. Jana, and T. Pal, "Biomolecule induced nanoparticle aggregation: effect of particle size on interparticle coupling," J. Colloid Interface Sci. **313**(2), 724–734 (2007).
38. S. Pramanik, P. Banerjee, A. Sarkar, and S. C. Bhattacharya, "Size-dependent interaction of gold nanoparticles with transport protein: a spectroscopic study," J. Lumin. **128**(12), 1969–1974 (2008).
39. K. F. Ren, G. Gréhan, and G. Gouesbet, "Radiation pressure forces exerted on a particle arbitrarily located in a gaussian beam by using the generalized Lorenz-Mie theory, and associated resonance effects," Opt. Commun. **108**(4-6), 343–354 (1994).
40. Y. Harada and T. Asakura, "Radiation forces on a dielectric sphere in the Rayleigh scattering regime," Opt. Commun. **124**(5-6), 529–541 (1996).
41. C. F. Bohren and D. F. Hufman, *Absorption and Scattering of Light by Small Particles* (Wiley, 1983).
42. A. Ashkin, "Forces of a single-beam gradient laser trap on a dielectric sphere in the ray optics regime," Biophys. J. **61**(2), 569–582 (1992).
43. C. Mätzler, "Matlab functions for mie scattering and absorption," (Research Report, Institut fur Angewandte Physik, University of Bern, Switzerland, 2002). *http://www.iapmw.unibe.ch/teaching/vorlesungen/radiative_transfer/HS2012/Mie_Version2.pdf*.
44. P. B. Johnson and R. W. Christy, "Optical constants of the noble metals," Phys. Rev. B **6**(12), 4370–4379 (1972).
45. A. N. Bashkatov and E. A. Genina, "Water refractive index in dependence on temperature and wavelength: a simple approximation," Proc. SPIE **5068**, 393–395 (2003).

46. F. Garcia-Santamaria, H. Miguez, M. Ibisate, F. Meseguer, and C. Lopez, "Refractive index properties of calcined silica submicrometer spheres," Langmuir **18**(5), 1942–1944 (2002).
47. Y. Seol, A. E. Carpenter, and T. T. Perkins, "Gold nanoparticles: enhanced optical trapping and sensitivity coupled with significant heating," Opt. Lett. **31**(16), 2429–2431 (2006).
48. P. V. Ruijgrok, N. R. Verhart, P. Zijlstra, A. L. Tchebotareva, and M. Orrit, "Brownian fluctuations and heating of an optically aligned gold nanorod," Phys. Rev. Lett. **107**(3), 037401 (2011).
49. Y. Hu, R. C. Fleming, and R. A. Drezek, "Optical properties of gold-silica-gold multilayer nanoshells," Opt. Express **16**(24), 19579–19591 (2008).
50. S. C. Padmanabhan, J. McGrath, M. Bardosova, and M. E. Pemble, "A facile method for the synthesis of highly monodisperse silica@gold@silica core–shell–shell particles and their use in the fabrication of three-dimensional metallodielectric photonic crystals," J. Mater. Chem. **22**(24), 11978–11987 (2012).
51. M. T. Kumara, N. Srividya, S. Muralidharan, and B. C. Tripp, "Bioengineered flagella protein nanotubes with cysteine loops: self-assembly and manipulation in an optical trap," Nano Lett. **6**(9), 2121–2129 (2006).

1. Introduction

Since the pioneer works by Ashkin and associates on optical levitation and tweezing [1], investigation on optical forces has known a tremendous development and is now considered as the corner stone of contactless manipulation techniques of small objects in fluid environments. Classically, optical tweezing takes advantage of opposing scattering and gradient forces to trap and move single particles [2,3]. The radiation pressure from scattering forces has also shown its efficiency in countering and balancing the Stokes drag for optical sorting and optical chromatography in order to separate flowing particles of different polarisabilities within microfluidic devices [4–7]. Up to now, most of the efforts have been devoted to describe these light couplings with model particles and to optimize light patterns for dedicated optical functionalities such as positioning [8], conveying [9], and sorting [10,11]. The manipulated particles were mainly pure dielectric or metallic [5,11–15], with sizes around the micrometer for dielectric particles and down to a few tens of nanometers for metallic particles [16,17]. The optical manipulation of cells [18], bacteria [19], pollens or spores [20], is also a very active field which has evidenced the importance of particle's internal complexity making difficult any attempt at quantitatively predicting the amplitude of the optical forces. This was our first motivation to investigate optical forces on microparticles with a controlled complexity [21]. The second motivation was to find a way to increase the amplitude of optical forces which is often too weak for applications. For instance the optical chromatography efficiency is limited in terms of particle downsizing due to the weakness of the scattering force amplitude compared to the Stokes drag; the actual limit being roughly the micrometer range for particle velocities of a few tens of μm/s under a 1W laser power [7]. Conversely, metallic particles exhibit much larger scattering cross sections than pure dielectric particles due to the presence of optical resonance in the visible spectrum, the so-called surface plasmon resonance (SPR), related to the dielectric confinement and imputable to the collective oscillations of the free electrons cloud. Such plasmon resonances in silica-metal raspberry and core-shell hybrid particles should increase the optical force amplitude and make their manipulation easier [11,12,22,23]. The third motivation to optically manipulate these hybrid dielectric-metal particles is related to the role they can play in several nanoscale promising applications: local sensing (hybrid particles allow enhanced sensitivity to their environment compared to single plasmonic particles) [24], electromagnetic field enhancement (silica-metal particles are promising SERS active probes) [25,26], and sub-wavelength optics (dielectric metal particles are used as elemental bricks for assembled meta-materials or as components in nano-devices) [27,28]. Nevertheless a quantitative description of optical forces on hybrid metal-dielectric particles still remains elusive but challenging even from a fundamental point of view.

Wet chemistry now allows the synthesis of a large diversity of particles [29,30], and particularly silica-gold raspberry-like particles [31,32]. From the material engineering point of view, these complex particles are very attractive as "micron-sized nanoparticles" because they present both micrometric size and nanoscale optical properties such as SPR [31,32]. They are also very striking systems because they are able to show how nanoscale tags can impact the mobility of microscale objects. Finally, these raspberries offer the opportunity to

investigate the role of increasing complexity in optical manipulation. The goal of the present work is to present quantitative results on the metallic contribution of the optical radiation pressure on silica-gold raspberries flowing in a microfluidic channel. We evidence a significant increase of the optical force magnitude compared to pure silica particles of the same overall size even at very low metal concentration (less than 1%). We also perform numerical simulation to quantitatively address the measured forces, and quantify the role of nanometric metallic tags. These results open up the way for the optofluidic actuation of hybrid plasmonic particles within microfluidic environments.

2. Experimental design

The experimental setup is based on the optical chromatography scheme illustrated in Fig. 1(a). We fabricate a microfluidic device using a 50 µm internal diameter cylindrical capillary (VitroCom). It is connected to a syringe pump or to a hydrostatic pressure control and then inserted in a water-filled quartz spectroscopy cell (Hellma) mounted on an Olympus IX71 inverted microscope allowing $\hat{x}$ and $\hat{y}$ displacements; $\hat{z}$ is the vertical axis. A continuous wave laser beam (wavelength in vacuum λ_0 = 532 nm from a Coherent Verdi Laser) with a single transverse mode and a Gaussian intensity profile is sent into the microchannel with a wave vector in the direction $-\hat{x}$ opposed to the fluid flow.

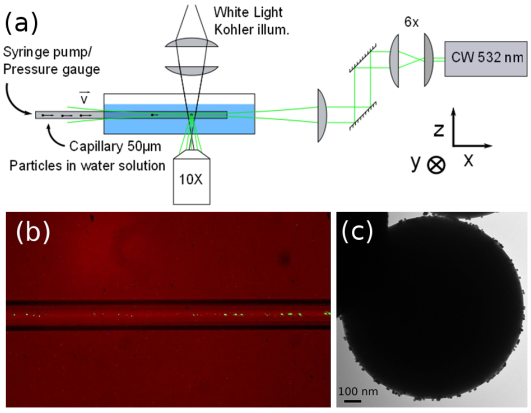

Fig. 1. (a) Scheme of the experimental chromatography setup. (b) Illustration of flowing particles in the microchannel; particles are magnified by the scattering of the green laser light (c) TEM image of a silica-gold raspberry particle with core diameter D = 1.17 µm and adsorbed gold nanosdots of diameter d = 15 nm (sample α, Table 1.).

The beam waist ω is set a few mm inside the microchannel exit at the center of the observation area of the microscope; it is controlled by a series of three fused silica lenses to be 15 µm large. Such a value ensures an overall coverage of the microchannel section by the transverse beam intensity distribution as it prevents diffraction effects by the microchannel edges. It also leads to a Rayleigh length of 1.4 mm, that allows to ignore the laser beam divergence over more than 2 mm centered around the beam waist by considering a mean beam waist ω = 17 ± 2 µm during the overall displacement of the particles. The two first lenses play the role of a telescope of magnification 6X and the third lens, of focal length 40 cm, loosely focuses the laser beam into the channel. Observation is performed with a 10X objective (Olympus UIS2 LMPLFLN) using both the white light Köhler source of the microscope and the green laser light scattered by the flowing particles; an orange band-pass filters allows to reduce the scattered intensity for naked eye observation and prevents camera saturation. Images, as that shown in Fig. 1(b), are grabbed at a frame rate of 5 fps with a USB camera mounted in place of one of the microscope eyepieces. The videos are analyzed with a homemade Matlab particle tracking program adapted from a free online code [33].

The particles are produced using a three-step method. First, we synthesize the silica microparticles with a constant monomer supply technique [34,35] to preserve monodispersity

during particle growth; the final size of the particles is monitored by the flow rate amplitude of a diluted tetraethyl orthosilicate solution. The particles are then characterized by Scanning Electron Microscopy (SEM) and Transmission Electron Microscopy (TEM). We choose two suspensions of average particle diameters, D = 1.17 µm and D = 1.46 µm with a standard deviation smaller than 3%, above the micron to guaranty optical actuation of pure silica particles with beam powers below the Watt. Gold nanodots were synthesized according to literature methods [36–38], yielding nanodots of diameter d = 15 ± 2 nm. Following the Pastoria-Santos method [31], the silica-gold raspberries are eventually assembled by performing a coating of the silica core with (3-aminopropyl)triethoxysilane (APS) and then by adding a determined volume of citrate stabilized gold nanodots that adsorb on the APS-coated silica surface. Assuming a perfect theoretical coverage of silica beads by 100% of the nanodots added in solution, concentrations are chosen so as to adsorb ~400 gold nanodots on a 1.17 µm-diameter particle (sample α, volume fraction for 100% yield $\phi_{100\%}$ = 1.1%) and ~250 and ~500 gold nanodots on a 1.46 µm-diameter particle (corresponding respectively to samples β and γ with volume fractions for for 100% yield $\phi_{100\%}$ of 0.45% and 0.9%); see Table 1. Figure 1(c) shows a TEM image of sample α, a raspberry with diameter D = 1.17 µm coated with d = 15 nm gold nanodots.

Table 1. Data on raspberries samples: diameter of the core silica microparticles, gold volume fraction $\phi_{100\%}$ estimated from quantities used in chemical synthesis, gold volume fraction ϕ deduced from cross section calculations and measured enhancement factor of optical forces compared to silica core

SiO_2@Au Raspberries samples	SiO_2 microparticle diameter D	Gold volume fraction $\phi_{100\%}$ (synthesis)	Experimental optical forces enhancement factor	Gold volume fraction ϕ (Mie calculation)
α	1.17 µm	1.1%	1.93	0.47%
β	1.46 µm	0.45%	1.39	0.20%
γ	1.46 µm	0.9%	1.83	0.43%

The samples are diluted to get 1.5 10^8 particles per mL in aqueous solution and infused in the microchannel with a 1.5 mL Terumo syringe. The flow is actuated either by a KD Scientific syringe pump or a pressure gauge. The first method, called optical chromatography mode, consists in establishing a controlled flow rate in the microchannel and using the counter-propagating electromagnetic wave to apply optical forces on the flowing particles in the opposite direction; particle are eventually immobilized when Stokes drag and optical radiation pressure are balanced. The second method, preferentially used in the present investigation is called velocimetry mode. It consists in initially immobilizing the particles within the microchannel by adjusting the hydrostatic pressure and setting them in movement by turning on the laser.

3. Theoretical aspects

Optical forces are related to momentum exchanges and/or transfer between the exciting electromagnetic wave and the irradiated particle. This occurs whenever the momentum of photons is modified in amplitude and/or in direction. For instance particles may be set in motion when they scatter photons elastically, a mechanism used in optical chromatography, or when photons are partially or totally absorbed by the particle. As a consequence, the momentum conservation produces a density force which is proportional to the wave momentum, $n I/c\,\hat{x}$, and to the radiation pressure particle cross section C_{rp} related to the scattering C_{scatt} and the absorption C_{abs} cross section; here I is the laser beam intensity, $\hat{x}$ the wave vector direction, n the index of refraction of the surrounding fluid and c the light celerity. The calculation of these cross sections is performed from the Generalized Lorentz Mie Theory [39,40]. Meanwhile, when the radius R of the particles is far smaller than the waist ω of the laser beam, as in the present experiments, one can consider the incident field as a plane wave and use the formalism of Mie Theory as described by Bohren and Huffman [41]. Mie theory calculation basically allows for the determination of C_{ext} (the so-called

extinction cross section) and C_{scatt}, and then $C_{abs} = C_{ext} - C_{scatt}$, from Mie wave amplitudes a_n and b_n involving Bessel functions and particle characteristics such as size and index of refraction (see [41] for details). In order to estimate the radiation pressure forces, one also needs to take into consideration the angular dependence of scattering by introducing the asymmetry parameter $g = \langle \cos\theta \rangle$, which gives the averaged scattering angle (incident wave direction $\theta = 0$, back scattering $\theta = \pi$) [41]. The force resulting from the interaction between the beam and the particle contains two contributions: one due to absorption, proportional to C_{abs}, and another one due to scattering $C_{scatt} \cdot (1 - \langle \cos\theta \rangle)$ to take angular dependence into account. The radiation pressure cross section is then the sum of these two terms: $C_{rp} = C_{abs} + C_{scatt} \cdot (1 - \langle \cos\theta \rangle)$. When the particle radius R is very small compared to the beam waist (*i.e.* $R/\omega << 1$), the plane wave approximation applies and the beam intensity distribution can be reduced to $I = 2P/\pi\omega^2$, where P is the laser beam power. The resulting radiation pressure force is: $F_{rp} = \frac{2P}{\pi\omega^2}\frac{n}{c}C_{rp}$. For convenience, we can also use the definition of the cross section efficiency $Q_{rp} = C_{rp}/\pi R^2$ to rewrite the force expression as:

$$F_{rp} = \frac{2P}{\pi\omega^2}\frac{n}{c}\pi R^2 Q_{rp} = 2P\frac{n}{c}\frac{R^2}{\omega^2}Q_{rp}. \quad (1)$$

At a given optical wavelength, we can consider two limiting particle size regimes: the Rayleigh regime for small particles (condition: $2\pi R << \lambda_0/n$) and the ray optics model for large particles (condition: $2\pi R(n_{part}/n - 1) >> \lambda_0/n$, where n_{part} is the refractive index of the particle). The latter is widely used in optical chromatography since this technique is mainly devoted to microparticles separation. In this case, Q_{rp} can be advantageously replaced by the ray optics efficiency Q* which only depends on the refractive indices n_{part} and n [7,42]. However when the size range of the used particles is close to the optical wavelength, a rigorous description of optical forces becomes mandatory and requires a Mie description of light scattering from Maxwell's equations. In this study, we performed calculations of F_{rp} within the framework of Mie theory for two main reasons. Firstly, the particles belong to a regime in between the Rayleigh and the ray optics one. Secondly, the Rayleigh and the ray optics formalism are not well-adapted to hybrid particles. For pure silica particles, we nonetheless performed Mie and ray optics calculations in order to compare them with previous works and to figure out the validity range of the approximation. For metal-dielectric particles, we calculated F_{rp} with a Matlab code implemented for spherical core-shell particles [43]. To do so, we need the dielectric functions of the core ε_{core} and the shell ε_{shell}. As the metal nanodots adsorbed on the silica microparticle surface are very small compared to the optical wavelength and since they are isotropically distributed onto this surface with a volume fraction ϕ around the percent, we can confidently assume a description of the shell as a continuous composite medium and use the Maxwell-Garnett approach to determine its dielectric constant:

$$\varepsilon_{shell} = \varepsilon_m \frac{\tilde{\varepsilon}(1+2\phi) + 2\varepsilon_m(1-\phi)}{\tilde{\varepsilon}(1-\phi) + \varepsilon_m(2+\phi)}, \quad (2)$$

with $\tilde{\varepsilon}$ the complex gold dielectric function derived from Johnson and Christy $\tilde{\varepsilon} = \varepsilon_{Au}(532\,\text{nm}) = -4.57 + i2.28$ [44], and ε_m the dielectric constant of the solvent $\varepsilon_m = \varepsilon_{H_2O} = n^2 = (1.335)^2$ at 20 °C [45]. The dielectric constant used for the core is taken

from measurements performed on similar silica particles $\varepsilon_{core} = \varepsilon_{SiO_2} = (1.425)^2$ [46]. The calculation of the cross-sections is performed using a Matlab code for core-shell particles with the previously mentioned dielectric constants.

The optical force F_{rp} is then estimated from measurements of the particle velocity υ and from the second Newton law, $F_{rp} + F_{Stokes} = 0$, where $F_{Stokes} = 6\pi R\eta|\upsilon|$ for a solid sphere and η is the water viscosity. However, the optical absorption of gold nanoparticles present in the shell of the raspberries will heat the surrounding water [47]. As a result, the viscosity of water will decrease as well as Stokes drag F_{Stokes} which varies linearly with η, and fitting the data without considering this issue may artificially increase the intrinsic enhancement of the optical force due to the gold layer. The temperature dependence of the viscosity of water can be estimated from the Vogel-Fulcher empiric law [48]. To calculate this overheating, we assume that neither silica nor water absorb light at the used wavelength. Using flux and temperature continuity conditions at both core/shell and shell/water interfaces, the absence of thermal gradient at the center of the particle and convergence to room temperature T_∞ at infinity, the stationary radial profile of temperature in water due to the thin composite shell is given by [47]:

$$T(r \geq R + d) = T_\infty + \frac{C_{abs} I}{4\pi\Lambda} \cdot \frac{1}{r}, \qquad (3)$$

where Λ is the thermal conductivity of water ($\Lambda = 0.6\ \mathrm{W.K^{-1}}.m^{-1}$). In our case the temperature increase $T(R+d) - T_\infty$ at the surface of the particles varies from 0 to 20 K, depending on the incident power and the volume fraction ϕ.

4. Results and discussion

To investigate the optical forces applied onto hybrid silica@gold raspberries in a microfluidic flow, we use the optical chromatography setup in the velocimetry mode illustrated in Figs. 1(a-b). The particles are initially immobilized within the microchannel by adjusting the hydrostatic pressure and then set in motion by turning on the laser. After a short time, the particles move at a constant speed, typically a few tens of μm/s depending on the laser beam power. We measure the particle velocity of both pure silica microparticles and silica@gold raspberries based on the same core particle. For pure silica microparticles, we deduce the optical force from a direct balance with the Stokes drag ($\eta_{H_2O} = 1.10^{-3}\ Pa.s$ at 20 °C). To measure the optical force enhancement induced by the metallic nanoparticles tags that partially cover the silica core (Fig. 1(c)), we proceed iteratively due to laser heating and the subsequent temperature dependence of the viscosity of water. Fixing the gold volume fraction ϕ, we first calculate the laser overheating and the water viscosity to get the Stokes drag and the enhancement factor on optical forces. Secondly, we use Mie theory to calculate the radiation pressure cross section C_{rp} of silica@gold raspberries, deduce the optical force and calculate the enhancement factor relatively to core particles. Dichotomy in volume fraction ϕ is performed up to equality of the enhancement factors. The converging gold volume fraction ϕ is finally compared to estimates from TEM images of the raspberries.

A typical snapshot illustrating particles in the microchannel is presented in Fig. 1(b). Figure 2 shows the time varying positions of silica-gold raspberries (Table 1, sample α, silica D = 1.17 μm, gold d = 15 nm) shined by the laser at the beam power P = 0.75 W. We performed linear fitting of at least 75 trajectories to measure an average velocity at a given laser power. The inset of Fig. 2 shows the velocity distribution obtained from this run with an average of 24 μm/s and a standard deviation of 6 μm/s. The trajectories being linear, this suggests that the particles remain in the Rayleigh zone where the field can be considered as almost axially uniform. Moreover, we observed that most particles move right in the center of

the microchannel. This effect is ascribed to two collaborating effects: (i) the weak shear associated to the Poiseuille flow velocity profile within the microchannel before stopping particles with pressure actuation and (ii) the presence of optical gradient forces due to the transverse Gaussian profile of the laser beam, as largely demonstrated in optical chromatography experiments [7,40].

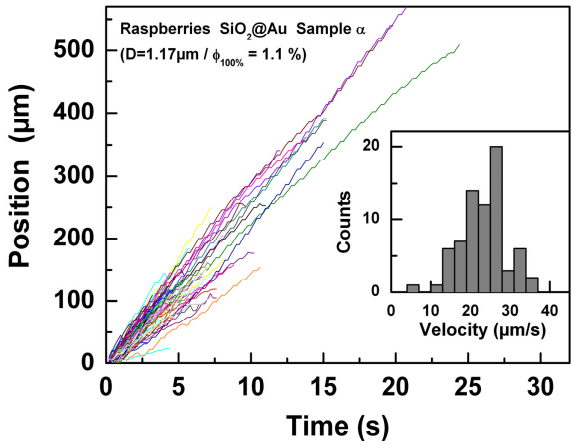

Fig. 2. Trajectories of 75 silica-gold raspberry particles (sample α, silica core diameter D = 1.17 µm coated by 15 nm gold nanodots) measured in the velocity mode as a function of time lapse for a laser beam of power P = 0.75 W and beam waist ω = 17 µm. The Inset shows the statistic distribution in particle velocity extracted from linear fitting of the trajectory set.

The measured velocity is directly related to the optical radiation forces applied to the particles. In such a low Reynolds number flow, equilibrium is rapidly set up between the optical and the drag force due to viscosity. For silica core particle, laser heating at the used wavelength can be discarded and we can derive forces easily. A linear fit of the experiments performed with D = 1.46 µm silica particles yields to a force of 0.36 pN/W. For particles with the smallest diameter, D = 1.17 µm, we measure a weaker force: 0.23 pN/W. The ratio of these two slopes, 1.57, is in very good agreement with the square of particle diameter ratio, as expected from the optical force expression given by Eq. (1).

To investigate the contribution of the gold nanodots on optical forces, we performed particle velocity measurements on suspensions with different silica core diameters and gold concentrations at the surface. Figure 3 shows a significant increase of the velocity for the silica microparticles coated with gold compared to that obtained for pure silica particles of same core diameter for both D = 1.17 µm (Fig. 3(a)) and D = 1.46 µm silica core diameter (Fig. 3(b)). We observe an enhancement of the velocity by a factor 2.34 for sample α, 1.55 for sample β and 2.31 for sample γ. This behavior is interpreted as a metal-induced enhancement of the radiation pressure cross section C_{rp}. Indeed, considering, on the one hand, the optical wavelength of the laser wave (λ_0 = 532 nm) and the SPR wavelength of 15 nm gold nanoparticles (λ_{SPR} = 525 nm) on the other hand, the presence of metal increases the scattering and absorption of the incident wave, increasing de facto radiation pressure forces [23].

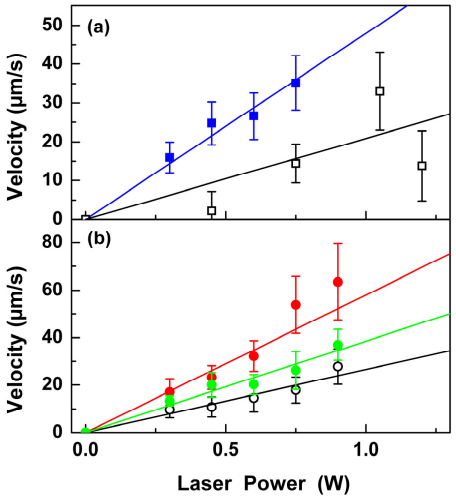

Fig. 3. Velocity as function of the incident laser beam power measured for different types of particles. (a) Core dielectric particles with a diameter of 1.17µm (black empty squares) and SiO_2@Au raspberries sample α (blue squares). (b) Core particles with a diameter of 1.46µm (black empty circles) and raspberries (green and red circles correspond to sample β and γ respectively). Error bars represent standard deviations. The linear fits are guides for the eye.

To estimate the amplitude of these enhancement factors, we performed numerical Mie calculations of the extinction, absorption, scattering cross section and the asymmetry parameter for our core-shell approach of silica@gold raspberry in order to obtain the gold volume fraction ϕ dependence of the radiation pressure cross section C_{rp}. Results are shown in Fig. 4 for D = 1.46 µm and d = 15 nm. The four colored curves correspond to the radiation pressure cross-section of dielectric-metal particles for ϕ = 0.2, 0.45, 1 and 2%. As expected, the radiation pressure cross section C_{rp} deeply increases when approaching the SPR, depending on ϕ, and then decreases to asymptotically collapse with the prediction for pure silica particles, in black. The comparison to pure silica particles at the used optical wavelength (indicated by the vertical dashed line) gives the theoretical variation of the expected enhancement factor versus the volume fraction ϕ of gold nanodots. The inset of Fig. 4 shows that the enhancement factor is linear in ϕ at low ϕ values.

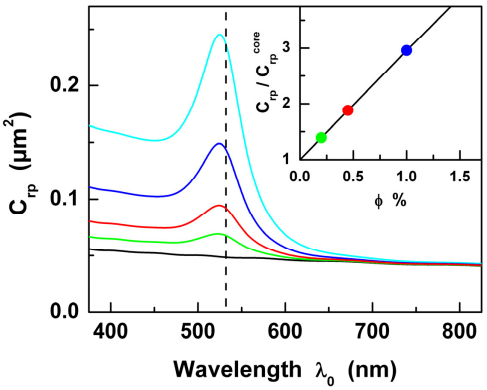

Fig. 4. Wavelength dependence of the radiation pressure cross section C_{rp} of silica-gold raspberries calculated using Mie theory for silica core diameter D = 1.46 µm, and d = 15 nm thick composite shell composed of water and gold nanodots with volume fraction ϕ = 0.20% (green), 0.45% (red), 1% (blue) and 2% (cyan). The behavior in black describes the silica core case. The vertical dashed line indicates the optical excitation wavelength of 532 nm. The Inset represents the evolution of the enhancement factor, *i.e.* the ratio of C_{rp} for raspberries over C_{rp}^{core} for silica core as a function of the metal volume fraction ϕ.

In order to estimate the radiation pressure forces experimentally, we have in the other hand to consider the temperature dependence of the viscosity within the Stokes drag expression and consequently the temperature at the vicinity of the particle which is directly related to the gold volume fraction of the shell. We proceed by dichotomy in volume fraction ϕ. This procedure is illustrated in Fig. 5. Given a value of ϕ, we calculate the absorbed power and the corresponding laser overheating (Fig. 5(a)), we deduce the water viscosity at the raspberry surface from the Vogel-Fulcher empiric law (Fig. 5(b)). We apply this procedure to the set of investigated laser powers and then we fit the experimental data with a linear law to get the slope F_{rp}/P (as in Fig. 5(d)). We then compare the enhancement factor on the force $(F_{rp}/P)/(F_{rp}/P)^{core}$ (relatively to measurements in silica core particles with same core diameter) to the numerically calculated one at the same ϕ. The process is iterated in ϕ up to equality between the two approaches (Fig. 5(c)). The optimal values of ϕ (enhancement factor matching) are summarized in Table 1 and Fig. 5(d) shows the final results for D = 1.46µm. For D = 1.17 µm (sample α) we deduce a force of 0.45 pN/W, giving rise to an enhancement factor of 1.93 compared to pure dielectric particles for ϕ = 0.47%. Moreover, as illustrated in Fig. 3(b) and Fig. 5(d), the optical forces are found to increase with the number of adsorbed gold nanoparticles. With silica particles of diameter D = 1.46 µm, we measure a force of 0.50 pN/W for the smallest gold volume fraction at the surface (sample β, green circles on Fig. 5(d)) and 0.66 pN/W for the largest one (sample γ, red circles on Fig. 5(d)), respectively corresponding to 1.39 and 1.83 enhancement factors (starting from the aforementioned 0.36 pN/W for pure silica core particles). Thus, one can estimate the metallic contribution to the total optical force. According to the dashed lines on Fig. 5(c), our procedure leads to gold volume fractions ϕ = 0.20% (sample β) and ϕ = 0.43% (sample γ).

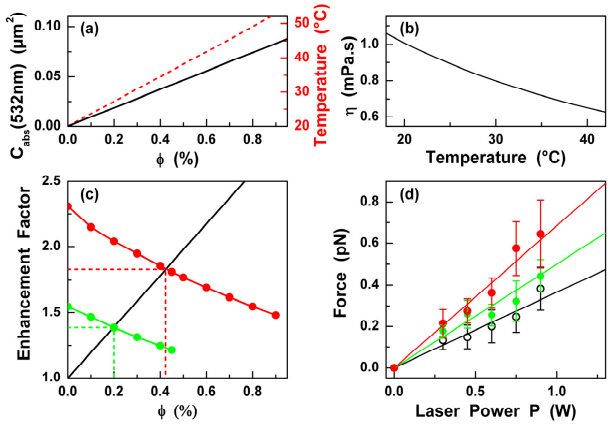

Fig. 5. (a) Absorption cross section of silica-gold raspberries at 532 nm using Mie theory for silica core diameter D = 1.46 µm, and d = 15 nm thick composite shell (gold and water) as a function of the volume fraction ϕ (black) and the corresponding temperature increase at the surface of the particle for a 1W laser illumination (red dotted line). (b) Temperature dependence of water viscosity estimated with the Vogel-Fulcher empiric law. (c) Evolution of the enhancement factor C_{rp}/C_{rp}^{core} as a function of the metal volume fraction ϕ using Mie calculations (black line) and from the experimental data (sample β in green and γ in red) considering the effect of temperature increase (from (a)) and temperature dependence of viscosity (from (b)). (d) Optical force variations as a function of the incident laser beam power P measured for core dielectric particles with D = 1.46µm (black empty circles), raspberries sample β (green circles) and sample γ (red circles).

The estimated volume fractions are almost half of $\phi_{100\%}$, those suggested from the synthesis with an expected 100% adsorption yield (Table 1). Similarly, the enhancement factor for the smallest silica core (D = 1.17 µm, sample α, Table 1) leads to a metal contribution ϕ = 0.47%. Note for instance that ϕ = 0.47% correspond to an inter-particle

distance of 156 nm which is compatible with a rough estimation made from geometric calculation on TEM images, Fig. 1(c), where we found a mean inter gold nanoparticles distance of 120 nm.

These volume fractions ϕ are finally used to estimate optical forces and compare them to absolute values calculated from Mie theory. In Fig. 6 we plot together the optical radiation pressure force predicted by Mie theory for the gold volume fraction ϕ obtained from the enhancement factor matching procedure and the set of optical forces measured for the various combinations of particles diameters and gold nanodot concentrations. Results on pure silica particles are also presented, including the force estimated in the ray optics approximation as it is used in most optical chromatography investigations [5,7,20]. The error bars associated to calculations (solely represented for pure silica) are estimated at ± 29% and originate from the beam waist $\delta\omega/\omega = 11\%$ and standard deviation of the radius of silica particles $\delta R/R < 3\%$. The error bars on experimental data points are estimated at ± 15% and originate from the standard deviation on R and the statistical error $\delta v/v = 12\%$ extracted from velocity measurements (Fig. 2). The error on ω seems large but it takes into account the fact that strictly speaking, particles do not flow along a perfect cylinder of light but in a slightly converging/diverging beam so that optical forces slightly vary along the beam axis. Consequently, agreement between Mie calculations of optical radiation forces and experimental measurements is fairly good; the largest data shift between predicted and measured forces is smaller than 25%, a value which has never been reached to the best of our knowledge, except by further adaption of the laser beam parameters [7]. Note nonetheless that experimental results are systematically over evaluated by Mie calculations; this is likely due to the internal porosity of Stöber like silica that randomly scatters light and thus reduces the force efficiency [46].

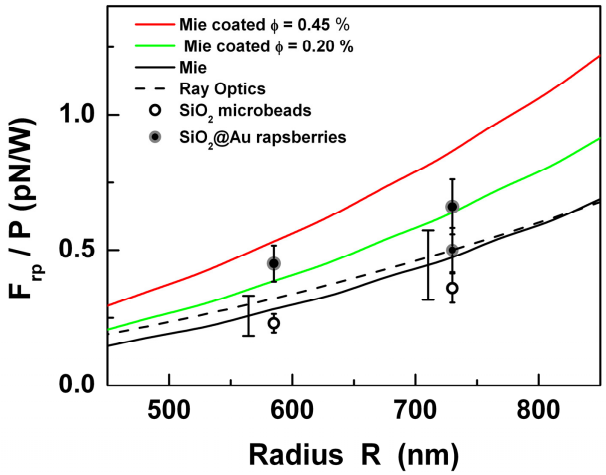

Fig. 6. Radiation pressure force variation versus the radius R of silica-gold raspberries predicted by Mie theory (red curve: ϕ = 0.45% as a mean between 0.43% (sample γ) and 0.47% (sample α), green curve: ϕ = 0.20%) and measured experimentally in the three raspberries samples (black-gray dots). Also shown for the comparison, are the calculation and measurements on core silica particles (black curve and empty circles respectively). The dashed curve represents the forces in the ray optics approximation for silica particles. Error bars also appear on calculations (just represented for silica particles for the sake of clearness) to take into account the weak beam size variation over the Rayleigh length during the particle displacement in the microchannel.

Finally, to compare with classical optical chromatography schemes [5,7], we present in Fig. 6 calculations in the ray optics approximation for silica particles in water, using already mentioned optical indexes. They fairly approximate Mie calculations for the investigated particle radii. They also show the robustness of this approximation beyond its size range

validity (here R ~λ_0 while R >> λ_0 would be required), and thus enlighten the traditional use of ray optics in optical chromatography. Thus, our results demonstrate that quantitative predictions can indeed be advanced for both core and much more complex core-shell micro materials when the Maxwell-Garnett formulation of the refractive index is applicable. Consequently, our experiments and calculations open the route for the study and the manipulation of hybrid particles with tunable optical properties such as multiple shell objects, micro-nano hybrids where nanometric tags present specific and tunable SPR [49,50], or complex engineered biological system [51].They also show the way to increase the magnitude of optical forces for particle actuation in microfluidic environments.

5. Conclusion

Using an optical chromatography setup, we investigated optical forces on dielectric core microparticles and hybrid dielectric-metal micro-nano raspberries based on the same silica core. We measured the enhancement of the optical force due to the metallic shell of the raspberries and found good quantitative agreement with a numerical simulation based on Mie theory. We also showed that even at very low metallic concentrations (down to 0.2%) we can definitively differentiate the particles through optical forces, thus demonstrating that nano metallic tags can significantly increase the magnitude of optical forces at the microscale. Consequently, using these “micron-sized nanoparticles”, one can associate ease of manipulation and benefit from nano-engineered materials used as tags where the micrometric range is dedicated to transportation and where the nanometric range offers specific and tunable optical, chemical or biological properties. These results also open up new opportunities in the field of plasmonic particles manipulation and sorting, as dielectric-metal microparticles could be easily differentiated according to their metal concentration in a very fine way. One can imagine using an optical chromatography setup to discriminate mixtures of inhomogeneously decorated particles and create ultra pure sets of similar raspberries with enhanced spectral properties.

Acknowledgments

The authors acknowledge the scientific program Advanced Materials in Aquitaine (GIS Matériaux) and the Conseil Régional d’Aquitaine (Project Nano-Trans N# 20111101010) for funding. The authors would also like to acknowledge networking support by the COST Actions MP 1202 (http://www.cost-hint.cnrs.fr) and MP 1205 (http://costmp1205.eu).